EXPERIMENTAL STUDIES OF ELECTRON COOLING

G. I. BUDKER, N. S. DIKANSKY, V. I. KUDELAINEN, I. N. MESHKOV,
V. V. PARCHOMCHUK, D. V. PESTRIKOV, A. N. SKRINSKY, B. N. SUKHINA

*Institute of Nuclear Physics, Siberian Division, USSR Academy of Sciences,
Novosibirsk 90, USSR*

Input of a beam of "cool" electrons into a straight-section orbit of a heavy charged-particle beam circulating in a storage ring introduces an effective friction when the velocities of heavy particles and electrons coincide in magnitude and direction. This friction causes the phase-space volume of the heavy-particle beam to decrease—"electron cooling."

In the work presented here, an experimental study was made of electron cooling of a beam of 35–80 MeV protons. A study was made of the electron-cooling effect on the proton lifetime in the storage ring. At a proton energy of 65 MeV and an electron current of 100 mA, the betatron-oscillation damping time was obtained and the equilibrium proton-beam dimensions were measured to be: diameter $\lesssim 0.8$ mm, angular spread $\lesssim 4 \times 10^{-5}$. Damping-time dependence on the parameters was also studied. The problem of the equilibrium value of the proton momentum spread is considered, and its experimental value is measured to be: $\Delta p/p \lesssim 1 \times 10^{-5}$.

A detailed description is given of methods for measurement of the proton-beam apertures.

Some possible applications of the electron-cooling method are described.

One of the main problems of particle storage rings is reducing the phase-space volume of a stored beam to provide multiple accumulation of particles. In electron-positron storage rings, this is possible due to synchrotron-radiation damping of particle oscillations. This paper concerns an electron cooling method which provides a possibility of multiple accumulation of heavy particles into the same phase space volume of a storage ring. The method was proposed by Budker and reported at the Colliding Beam Symposium in 1966.[1]

In electron cooling, a beam of electrons is introduced into one of the straight sections of a heavy-particle storage ring with a mean velocity equal in magnitude and direction to that of the heavy particles. Coulomb scattering leads to energy exchange between the two kinds of particles and, if the electron beam is monochromatic enough and the particle trajectories are parallel, the electron beam will play the role of a "cooler", absorbing the excess energy of the "hot gas" of heavy particles. In a coordinate system moving with the mean particle velocity, such a mixture of two beams passing through each other is similar to a two-component plasma relaxing until the temperature values become equal.

The main characteristics of the electron-cooling process are considered theoretically in Refs. 1 to 4.

The method of obtaining a cooled beam will be quite different for various ranges of particle energies. For proton energies up to 1 GeV (500-keV electrons), the most simple and natural seems to be a scheme with direct acceleration of electrons and subsequent recovery of their energy. For energies sufficiently high (20 GeV for protons, 10 MeV and higher for electrons), one will have to use an electron storage ring as an electron "cooler" in which beam monochromatization is achieved by synchrotron radiation.[4] Finally, in the intermediate region it seems possible to explore a scheme with a circulating beam. Electrons are removed from the circulating beam after being "heated" and replaced with a new beam of cooled electrons, thus making use of the electron-beam heat capacity.

In the work presented here, experimental results are described on electron cooling of a proton beam. The experiments were carried out in 1974–75. Some of them have been described earlier,[5,6] but for the sake of completeness, the most important results are included in this paper.

Electron cooling enables one to perform a multi-turn stacking of heavy particles. Estimates show that using this method, one can stack intense antiproton beams to provide a colliding-beam luminosity of as much as 10^{31} cm^{-2} sec^{-1}.

Two other proposals for stacking antiprotons are known to us. In the first,[7] it is proposed to stack antiprotons resulting from decay in the storage-ring chamber of $\bar{\Lambda}^0$ hyperons produced on an internal target by protons accelerated in the

CPS synchrotron. The efficiency of this method is quite low and the expected luminosity is about 10^{25} cm^{-2} sec^{-1}.

The second proposal is based on the so-called stochastic-damping method of betatron oscillations[8] suggested by C. van der Meer in 1972. This method has not been sufficiently studied yet and the experimental results available[9] do not enable one, in our opinion, to make definite evaluations of its advantages.

Electron cooling, apart from its main purpose as a method of achieving multiturn stacking of intense heavy-particle beams, may find application in a number of other experimental setups.

I EXPERIMENTAL SETUP

The experiments of the electron-cooling study were carried out on the storage ring NAP-M (Figure 1) specially designed for this purpose. Detailed descriptions of the storage ring are given in earlier papers.[10-14]
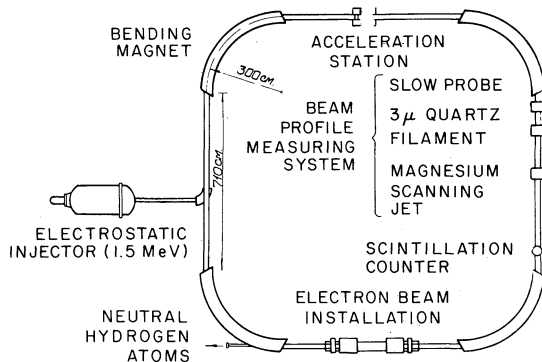

FIGURE 1   Layout of the proton accelerator NAP-M.

NAP-M is a zero-gradient racetrack synchrotron with edge focusing. Quadrupoles placed at the straight-section ends permit correction of the betatron tune shift.

Injection is from a 1.5-MeV electrostatic generator with proton current 1.5 mA per pulse; injection-pulse duration 4 μsec; emittance 0.15 πmrad-cm.

The electron-beam device[15] is located in one of the storage-ring straight sections; its parameters are given in Table II, and its layout is shown in Figure 2.

For electron-beam formation and transport, a homogeneous longitudinal magnetic field is used

TABLE I

Main parameters of the storage ring NAP-M

Proton energy	up to 150 MeV
Injection energy	1.5 MeV
Curvature radius in magnets	3 m
Straight-section length	7.1 m
Vacuum-chamber dimensions in magnets	
vertical	± 3.5 cm
radial	± 5 cm
Cooling-section aperture	± 5 cm
Betatron wave numbers	1.24, 1.34
Floquet-function values	
in cooling section	0.7
on the straight-section edges	0.98
ψ-function values in the straight section	0.8
Transition energy	110 MeV
Acceleration-cycle duration	30 sec
Average pressure	5×10^{-10} Torr
Vacuum chamber is heatable	(T approximately 300°)

TABLE II

Parameters of the electron-beam device

Cooling-section length	1 m
Electron energy	up to 100 keV
Electron current	up to 1 A
Electron angular spread θ_e	2×10^{-3}
Longitudinal magnetic field	1 kG

at the gun location, designed to give particular optical properties.[16] The magnetic-field homogeneity is kept at a relative level of 3×10^{-3} by means of magnetic shields and correcting coils. The device has three straight sections, in two of which guns and collectors are placed. The third is built into the straight section of the proton storage rings (interaction region). The straight sections are connected by means of two sections used for the input of electrons into the interaction section and for their output. The centrifugal drift of electrons is cancelled by
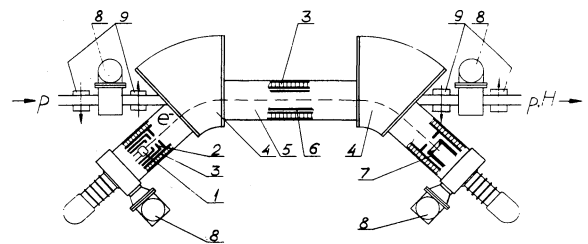

FIGURE 2   Layout of the electron-beam device: 1—electron gun; 2—anodes; 3—solenoids; 4—bending sections of electron beam; 5—cooling section; 6—vacuum chamber; 7—collector; 8—vacuum pumps, 9—correction magnets.

adding a transverse magnetic field, leading electrons along trajectories that coincide with longitudinal-field lines of force.

Typical operation of the device is as follows. Protons are injected into a rising magnetic field. Injection timing is synchronized with the field level by an NMR sensor with accuracy $\Delta H/H \lesssim 10^{-4}$. With the same relative accuracy, the peak value of the magnetic field is detected, giving the momentum of accelerated protons. When operating, the currents in bending magnets and correcting coils are under computer control. As the desired proton energy is reached, the magnetic-field rise is stopped, the rf system is turned off, and protons coast in a constant magnetic field with stability on the level of $\Delta H/H \lesssim 1 \times 10^{-4}$ during the experiment. For frequencies higher than 4 Hz, the ripple level does not exceed 1×10^{-5}. After switching the rf system off, the electron-beam device is fired up: longitudinal magnetic field, electron heating of the gun cathode and the proper current of electrons are established (high voltages for a gun and a collector are initially applied and are only retuned when the experimental energy is changed). Electron energy in the experiments was stabilized with an accuracy of 5×10^{-5}; the longitudinal magnetic field stability was better than 5×10^{-4}.

II MEASUREMENTS OF PROTON-BEAM PARAMETERS

A Measurements of Coasting-Proton Current

Measurements of coasting-proton current were performed by means of a magnetometer[17] which detects the magnetic field of the beam. The magnetometer sensitivity is about 5 μA and measurement time is about 1 sec in the current range .5–100 μA. Bunched-beam current was measured by an integral pick-up electrode and a Rogovsky coil.

B Aperture Probes

For measurements of the proton beam dimensions and position, aperture probes crossing the beam at a low velocity were employed. This method has quite high sensitivity if scintillation counters are used to detect protons scattered at a small angle by the probe edge. In the experiments, the counter and probe are located at the opposite ends of a straight section (Figure 1). The method's resolution $2a_{\min}$ is determined by the probe velocity v_{pr}. Without electron cooling, multiple scattering of protons by the residual gas atoms causes proton-beam enlarging. The time rate of change of the square of the beam radius a is given by

$$\frac{da^2}{dt} = \frac{b^2}{\tau_0}, \tag{1}$$

where τ_0 is the beam lifetime for the full aperture of the storage ring; b^2 is a constant. Then, from the obvious requirement that the change in a^2 from multiple scattering be small compared with the resolution,

$$\Delta a^2 = \frac{da^2}{dt} \cdot \frac{a_{\min}}{v_{pr}} \ll a_{\min}^2$$

follows

$$a_{\min} \simeq \frac{b^2}{v_{pr} \tau_0}. \tag{2}$$

When there is electron cooling and the proton-beam equilibrium dimensions are achieved (see Section V), Eq. (2) remains valid if τ_0 is replaced by τ_{ss}, the lifetime of protons again single scattering (see Section IV).

For typical conditions of the experiment ($\tau_0 \simeq 10^3$ sec, $\tau_{ss} = 5 \times 10^3$ sec) and the probe velocity 0.3 cm/sec, the estimate of Eq. (2) gives 0.1 and 0.02 mm, respectively. Thus, the method's resolution is determined in practice by what is technically possible (accuracy and homogeneity of the probe velocity, the frame skew etc.), which enable one to provide a resolution of the order of 0.1 mm.

C The Crossing-Filament Method

A thin quartz filament crossing the beam with high enough velocity, in contrast to the previous method, enables one to measure the proton density distribution without destruction of the beam. The sensor is designed as a frame, one side of which is fixed on a steel wire 1.6 mm in diameter (Figure 3). On the opposite side of a frame the thin quartz filament 2–3 μm in diameter is fixed. The frame can perform rotational oscillations with frequency of 40 Hz around the axis of the wire. In the two terminal positions (oscillator stop points), the frame position is fixed by means of electromagnets. The suspension-mechanism adjustment was performed in such a way that the filament in its equilibrium state should be on the equilibrium orbit. Then the
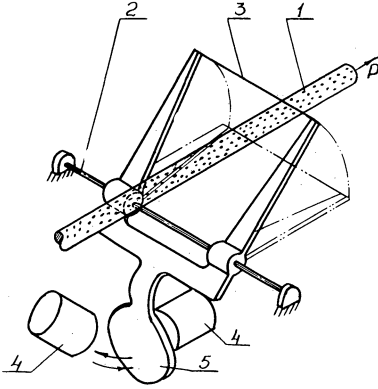
FIGURE 3 Proton beam-density measurements system (crossing-filament method): 1—proton beam; 2—steel wire; 3—quartz filament; 4—clamping electromagnets; 5—anchor.

section with the maximum filament velocity corresponds to the instant of a beam crossing. A single crossing is attained by switching the electromagnets off for the time required for the frame to pass from one terminal point to the other.

Detection of protons scattered by a filament was performed similarly to that in the probe method described above.

Protons scattered by the filament form a "halo" around the unscattered beam. As a result, the signal obtained when the filament crosses the beam is the sum of a signal from the initial particle distribution and a signal from the "halo" appearing with the beam-filament crossing.

The ratio of the signal from the halo to the initial-distribution signal is the same as the ratio between the beam density and the density of particles forming the halo. The particle density in the halo one can evaluate as follows:

The rms oscillation amplitude increment for a proton from a single pass through the filament is determined by

$$\Delta = \sqrt{\langle \Delta z^2 \rangle} = R_0 |f| \sqrt{\frac{2\Delta\theta_z^2 d}{\pi}}, \qquad (3)$$

where $\Delta\theta_z$ is the rms scattering angle of a proton per unit length in the filament material, d is the filament diameter, R_0 is the average radius of the storage ring, and $|f|$ is the value of the Floquet function at the point of the filament location. The proton scattering probability on the filament at a single crossing of the beams is

$$\varepsilon = 1 - \exp\left(-\frac{d}{v_w T_s}\right), \quad d \ll a_0, \qquad (4)$$

where v_w is the filament velocity, T_s is the particle revolution period, and a_0 is the proton-beam dimension. The density of particles forming the halo is of the order $\varepsilon N/(\Delta^2 + a_0^2)^{1/2}$ and the ratio of a signal from the halo to the useful signal $V \sim N/a_0$ is

$$\frac{\Delta V}{V} = \frac{\varepsilon a_0}{\sqrt{\Delta^2 + a_0^2}}. \qquad (5)$$

If the particle oscillation-amplitude increment is appreciably less than the aperture and the filament velocity is high enough to be able to ignore multiple passes of particles through the filament ($\varepsilon \ll 1$), the beam losses are then determined only by the single scatterings at angles larger than that of the aperture. At a proton energy 65 MeV, the increment of betatron-oscillation amplitude for the quartz filament of 2 μm in diameter moving with a speed of 5.5 m/sec is 3 mm, the scattering probability $\varepsilon = 0.55$, so that in measuring a beam of diameter 2 $a_0 = 1$ mm, the halo contribution is no larger than 10%. The halo presence is easily seen in the oscillograms of a signal shown in Figure 4. The halo contribution, according to Eq. (5), decreases as the proton beam dimensions reduce. An interesting feature of the method described is that its resolution capability is approximately the same as the filament diameter. There are also errors arising from filament skew or proton median-plane skew with respect to the geometrical axis of the storage ring. In this case the degree of freedom are "intermixed." These effects restrict the possibilities of independent measurements of the beam transversal dimensions.

D Magnesium-Jet Method

The magnesium-jet method[18] is based on detection of electron ionization occurring when the proton beam is crossed by a vapor jet. In the experiments a band jet was employed with transverse dimensions 1×20 mm^2, the vapor pressure being about 10^{-6} Torr. A container with the magnesium is heated up to a temperature of 450°C. Magnesium vapor is emitted through a number of holes 0.5 mm in diameter located on one of the container walls (Figure 5). For the final collimation of the jet, a shield is located 40 mm from the container wall. The container and the collimator are fixed on a rod that moves vertically with velocity 0.3 cm/sec within the range ± 3 cm, which enables one to
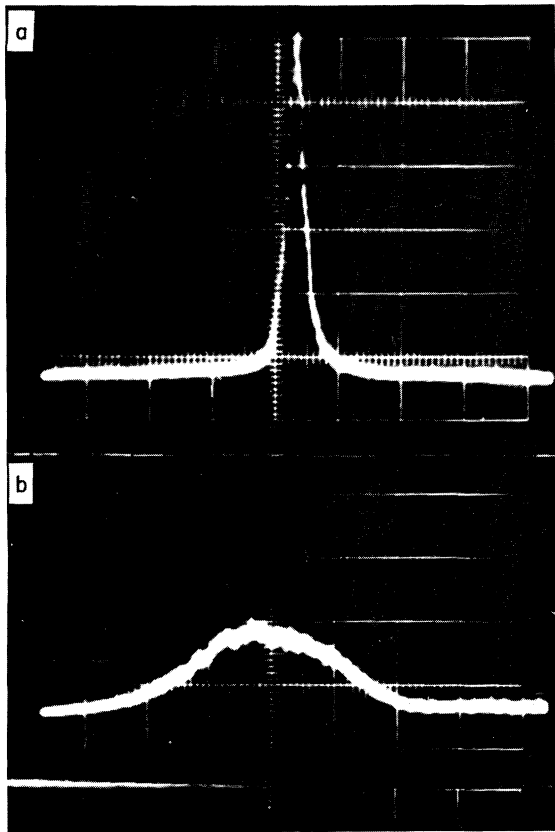
FIGURE 4 Vertical distribution of the proton-beam density (crossing-filament method). Scanning scale 5.5 mm/div. a—electron cooling is on; electron current 100 mA, proton energy 65 MeV, equilibrium dimensions 1.4 mm; b—electron cooling is off, beam 200 sec after acceleration.
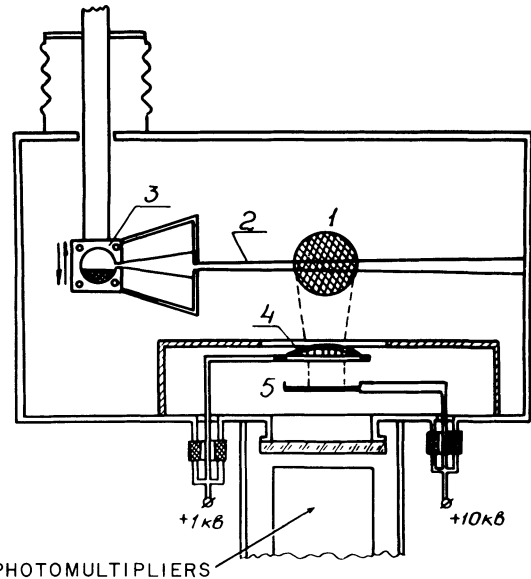

PHOTOMULTIPLIERS

FIGURE 5 Proton beam-density measurement system (magnesium-jet method): 1—proton beam; 2—magnesium jet; 3—magnesium container; 4—collector; 5—luminophore screen.

"observe" the whole useful aperture with the magnesium jet. Ionization electrons are collected by an electric field on a luminophore with an applied potential of +10 kV (preacceleration). Luminophore luminescence is detected by photomultipliers. Oscillograms of the photomultiplier signals obtained with proton-beam scanning are given in Figure 6.

The choice of magnesium as operating material was determined by the necessity to provide an average pressure in the storage ring on the level 5×10^{-10} Torr with quite a high-density jet. Metal-vapor condensation of the chamber walls facilitates this task substantially. The relatively low sublimation temperature of magnesium, its low chemical activity at temperature 450°C, as well as the lack of need for special care for its use all make

magnesium preferable to other light metals (lithium, beryllium).

In spite of the low resolution ($\Delta z \simeq 0.5$ mm), the method described advantageously supplements the crossing-filament method previously described and is very convenient for measurements of large beam dimensions and for operational running of a cooling process, as well as for the study of the time characteristics of oscillation damping.

With vertical scanning, a signal from the photomultiplier is proportional to the number of protons in a given horizontal cross section of the beam (Figure 6). Therefore, by shifting the jet along the coordinate z, one can obtain the proton distribution along the coordinate. If the jet is fixed at a certain point z, one is able to measure the proton density variation with time in a z-cross section of a beam. This method was employed in the experiments for measurements of the oscillation damping decrement. The magnesium jet was put in a position corresponding to the maximum density of a cooled beam. After that, proton oscillations in the beam were excited by a deflector kick and simultaneously the oscilloscope scanning was triggered (Figure 7). The signal peak at the initial moment corresponds to the proton density reduction in the beam center just after the kick; the further behavior of the signal demonstrates the beam contraction and the particle-density increase. The
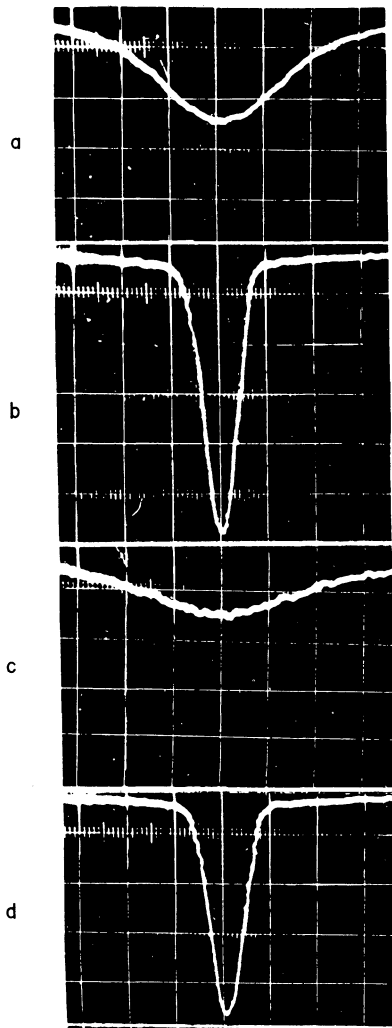
FIGURE 6   Vertical distribution of the proton-beam density (magnesium-jet method). Scanning scale 1 mm/div. a—proton beam just after acceleration; b—cooled beam, electron current 100 mA, equilibrium dimension 0.8 mm; c—the beam 2 min after acceleration, cooling is off; d—electron cooling is switched on 2 min after acceleration; the beam shown in Figure 6(c) is cooled.

signal from the photomultiplier varies according to the law:

$$
V(t) = V_0 \begin{cases} 1 & , \quad t < 0 \\[2mm] \sqrt{\dfrac{(a_z^2)_{\min}}{(a_z^2)_{\min} + B^2 \exp(-2\lambda t)}}, & t > 0 \end{cases} \tag{6}
$$

In the experiments, the photomultiplier signal was analyzed with a computer least-squares method to find the required parameters $a_{\min}^2$, B^2, λ.
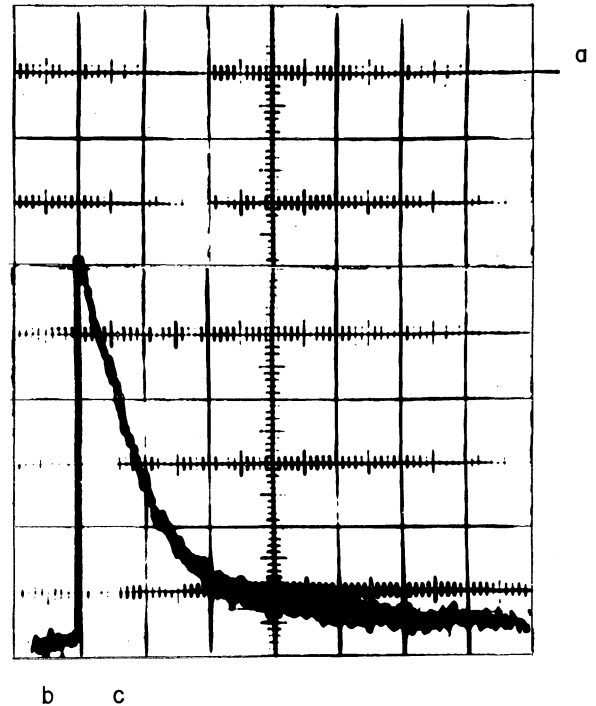

FIGURE 7   Proton beam-density variation in the center of the beam after the inflector kick. Scanning scale 2 sec/div. a—signal level out of the beam; b—the signal with the jet at the center of the beam prior to the inflector kick; c—the same signal after the inflector kick.

E   Method of Neutral Hydrogen Atoms

With a small difference between velocities of protons and electrons ($\Delta v/v \lesssim 10^{-3}$) in the cooling section, radiative recombination of protons and electrons is observed, with neutral-hydrogen atom production. These atoms, having energies like that of protons in the lower excited and main states, are not ionized by the storage-ring magnetic field (the electric field in the particle system is 400 kV/cm) and are therefore not deflected. The atoms are brought outside through a special window in a vacuum chamber made of stainless-steel foil 0.2 mm thick (Figure 1). A telescope made of scintillation counters and a two-coordinate proportional wire chamber detects both the full flux and the profile of a beam of neutral atoms (in practice, of course, protons are detected, when they appear in "stripping" the neutral atoms on the output window foil). In this way, one can measure the angular spread of the proton beam in the cooling section by using the long distance from the production point to that of observation.

III PROTON BEAM WITH ELECTRON COOLING

The main results in the experiments are the following. If the proton and electron velocities are the same in magnitude and direction with an accuracy $\Delta v/v \lesssim 1 \times 10^{-3}$ we observe:

i) betatron-oscillation damping;

ii) existence of an equilibrium dimension for a proton beam;

iii) energy-spread reduction in a proton beam and "blowing off" (acceleration or deceleration) of protons caused by electrons;

iv) substantial increase of the proton lifetimes.

If the difference between the proton and electron velocities $\Delta v/v$ is larger than 2×10^{-3}, these effects are eliminated. The experiments were carried out with the unbunched beam in the proton energy range 35–80 MeV. A study of the bunched-beam cooling has not been performed because of the small lifetime τ_{rf} of a beam with the rf system on: the noise of the storage-ring bending field and the noise of the rf system do not permit one to obtain τ_{rf} values substantially higher than 100 sec. Now, by lowering the noise level we have succeeded in increasing the lifetime up to 1000 sec, which enables one to carry out further experiments on the bunched-beam cooling.

The main results of the experiments on cooling the coasting proton beam are given in Table III. The effective electron temperature T_e given in Table III is derived from the equilibrium vertical

TABLE III

Typical experimental parameters and results of proton cooling

Proton energy	35–80 MeV
Electron energy	19–43.6 keV
Electron beam diameter	10 mm
Electron current I_e	0.1–0.25 A
Proton current I_p	20–100 μA
Average pressure	5×10^{-10} Torr
At an energy 65 MeV	
Equilibrium dimensions of proton beam	0.8 mm
Cooling time (at electron current 0.1 A)	5 sec
Lifetime in cooling regime	5000 sec
Lifetime without cooling	900 sec
Effective electron temperature T_e	0.2 eV
Neutral hydrogen atom flux	
$I_e^{-1} I_p^{-1} \dfrac{dN}{dt}$	17 ± 2 A^{-1}A^{-1}sec^{-1}

dimension of the proton beam (Section V). Estimates made on the basis of measurements of other characteristics give close values of T_e (Sections VI and VII).

IV LIFETIME OF PROTONS

The lifetime of protons coasting in the storage ring depends on many factors, among which one should note primarily the effects of resonances and perturbations of the magnetic system, effects of space charge and perturbing effect of magnetic-field noise and interaction with the residual gas. In the experiments being described the latter was dominant.

Multiple scattering of protons on the residual gas without damping causes a slow (diffusion) increase of amplitudes of betatron oscillations and, consequently, beam expansion up to the aperture dimensions with subsequent particle losses on the vacuum-chamber walls. This process is characterized by a time constant τ_{ms}. Single Coulomb scattering (nuclear scattering at this energy is negligible) at an angle larger than that of the aperture leads to the particle disappearing however small the beam dimensions are, and the beam intensity reduces with the time constant τ_{ss}:[19]

$$\tau_{ss} = \left(\frac{b}{R_0}\right)^2 \frac{\beta^3 \gamma^2 M^2 c^3}{4\pi\, Z^2 e^4 n_A \langle |f|^2 \rangle |f|^2_{\max}} \simeq L_Z \tau_{ms}.$$

(7)

Here, b, R_0 are respectively the aperture and mean radius of the storage ring; f is the Floquet function for the storage ring; β is the proton equilibrium velocity in units of the speed of light c, $\gamma = (1 - \beta^2)^{-1/2}$; e, M, m are respectively the charge and mass of a proton and electron; Z, n_A are the atomic number and the atom density of the residual gas, $L_Z = \ln(133 Z^{-1/3})$ is the Coulomb logarithm for the scattering process on nuclei, $\langle\ \rangle$ means averaging over the orbit.

Ionization losses reduce the proton mean energy, resulting in reduction with time of the equilibrium-orbit bending radius:

$$R(t) = R(0) - b\frac{t}{\tau_\varepsilon}$$

$$\tau_\varepsilon = \frac{b}{R_0} \frac{\beta^3 \gamma m M c^3}{4\pi Z e^4 n_A \psi_{\max}} \left[\ln\left(\frac{2\beta^2 \gamma^2 m c^2}{I}\right) - \beta^2\right]^{-1}$$

(8)

Here I is the average ionization potential of an atom and ψ_{max} is the maximum value of the ψ function for the storage ring.

Fluctuations of ionizational losses enlarge the energy spread in a proton beam, which leads to its (diffusional) radial-dimension expansion.

The lifetime of a proton beam can be roughly estimated from the partial times τ_{ss}, τ_{ms}, and τ_ε. For the parameters of the installation NAP-M $A_{eff} = 2$ cm, vacuum 5×10^{-10} Torr, $Z = 7$, $\beta = 0.35$; the corresponding quantities have the values: $\tau_{ss} = 7 \times 10^3$ sec, $\tau_{ms} = 1.5 \times 10^3$ sec, $\tau_\varepsilon = 2.5 \times 10^3$ sec, which gives a lifetime of order 1000 sec. The values are consistent with the experimental results given in Table III.

If the electron cooling acts effectively, the oscillation damping of protons introduced by electron cooling causes beam contraction and suppresses the expansion due to multiple scattering and the proton acceleration by electrons counteracts the ionization energy losses of protons. As a result, the lifetime of protons in the cooling regime is determined by the value of τ_{ss}. The concepts given are clearly demonstrated in Figure 8. Without electron cooling (curve 1), the proton beam with dimensions (just after acceleration) appreciably less than the aperture grows slowly at first, and its intensity is reduced only by single scattering with the time constant τ_{ss} (the "plateau" on the curve 1). After the beam grows up to the aperture dimensions, its intensity is reduced with the time constant $\tau_{ms} \simeq 0.2\ \tau_{ss}$. With electron cooling, the beam does not grow, and its intensity is reduced with the time constant τ_{ss} (curve 2) and consequently the lifetime increases by a factor of $I_z \simeq 5$. This lifetime increase for the proton beam was the first effect observed in experiments on electron cooling.

V EQUILIBRIUM AMPLITUDES OF BETATRON OSCILLATIONS

The proton-beam contraction and its monochromatization in the cooling regime proceed when damping dominates over diffusion processes. The latter, apart from multiple scattering and fluctuations of ionization losses, comprise the proton diffusion caused by the noncoherent fluctuations of the electron-beam density, by noise of power supplies for the electron beam or for the magnetic field of the storage ring, etc. The corresponding balance equation (Langevin equation) for the square of the betatron-oscillation amplitude of the
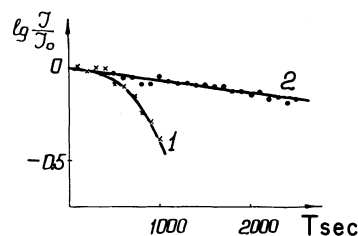

FIGURE 8   Time dependence of the proton-beam current: 1—without electron cooling; 2 -with electron cooling. Proton energy 65 MeV electron current 100 mA.

i-th coordinate has the form:

$$\frac{dA_i^2}{dt} = -\frac{2A_i^2}{\tau_e} + \sum_K \left(\frac{dA_i^2}{dt}\right)_K, \qquad (9)$$

where τ_e is the cooling time for small amplitudes and $(dA_i^2/dt)_K$ is the diffusion rate for the corresponding process. In particular, for multiple scattering

$$\left(\frac{dA_i^2}{dt}\right)_{ms} \simeq \frac{2b^2}{\tau_{ms}}. \qquad (10)$$

In the simplest case, when the electron-beam density is constant and electrons have a spherically symmetric Maxwell distribution in the velocities, analytical expressions [Eqs. (11–14) and Eq. (17)] can be obtained describing the betatron-oscillation damping caused by electron cooling. A nonspherical distribution does not significantly alter this relation. For proton diffusion on electrons of a cooling beam[2,20]

$$\left(\frac{dA_i^2}{dt}\right)_e = \frac{4m}{M}\frac{R_0\theta_{ei}^2}{\tau_e}\langle|f_i|^2\rangle_e, \qquad (11)$$

where θ_{ei} is the rms value of the ratio of the i-th transversal component velocity to the average velocity and $\langle|f_i|^2\rangle_e$ is an average taken over the cooling section for the Floquet function for the i-th degree of freedom.

Equilibrium values for the amplitudes A_{eq} can be derived by setting the right-hand side of Eq. (9) to zero. For the most important diffusion processes [Eqs. (10 and 11)], we obtain

$$\frac{A_{eq}}{R_0} =$$

$$\sqrt{2\frac{m}{M}}\ \theta_{ei}\sqrt{\langle|f_i|^2\rangle_e + \frac{M}{2m}\left(\frac{b}{R_0\theta_{ei}}\right)^2\frac{\tau_e}{\tau_{ms}}\langle|f_i|^2\rangle}. \qquad (12)$$

In the case of sufficiently low pressure, when

$$\tau_{ms} \gg \frac{M}{2m}\left(\frac{b}{R_0\theta_{ei}}\right)^2 \frac{\langle|f_i|^2\rangle}{\langle|f_i|^2\rangle_e}\tau_e, \qquad (13)$$

equilibrium amplitude values are achieved that correspond to having the "temperatures" of the electron and proton "gases" equal, the so-called "temperature limit" for the proton-beam dimensions:

$$\frac{A_{eq}}{R_0} = \sqrt{2\frac{m}{M}\langle|f_i|^2\rangle}\,\theta_{ei} \qquad (14)$$

In the experiments, the minimum vertical and radial dimensions of a proton beam are found to be 0.8 mm ($A_{eq} = 0.4$ mm). Formula (12), using the measured value A_{eq}, gives $\theta_{ez} = 1.5 \times 10^{-3}$ or $T_e = 0.2$ eV. It is interesting that the proton-beam dimension is only twice as large as the temperature-limit value (14) obtained for this θ_{ez}.

VI DAMPING DECREMENTS OF BETATRON OSCILLATIONS

For small amplitudes of betatron oscillations, when the rms proton velocity in the particle system is less than the rms velocity of the electrons or, in the laboratory system, when

$$\theta_{pi} < \theta_{ei}, \qquad (15)$$

the frictional force is proportional to the proton velocity[1] and one can introduce the damping decrement of oscillations or the cooling time for small amplitudes

$$\lambda_i = -\frac{1}{2M}\frac{\partial F_i}{\partial v_i} = \tau_e^{-1}. \qquad (16)$$

In the case of a constant density of the electron beam and a Maxwell distribution of the electron velocities, an expression for τ_e has the form

$$\tau_e = \frac{3}{2\sqrt{2\pi}}\frac{\beta\gamma^2}{cr_p\eta L_p}\frac{mc^3}{ej}\left(\frac{T_e}{mc^2}\right)^{3/2}, \qquad (17)$$

$$T_e = \beta^2\gamma^2 mc^2\theta_{ei}^2, \qquad (18)$$

where η is the fraction of the proton orbit occupied by the electron beam, $L_p \simeq 20$ is the Coulomb logarithm for the scattering of protons by electrons, r_p is the classical radius of the proton, j is the electron current density, and T_e is the electron temperature in the particle system. Formula (17) does not take into account the effect of a longitudinal magnetic field on the transition of proton energy to electrons caused by interactions, so that is justified only for transverse proton oscillations.

In the experiments, the damping decrement of vertical oscillations was measured and its dependence of various parameters was studied. Measurements were carried out using the method described in Section II (magnesium-jet method). In the initially cooled ($A_{eq} = 0.4$ mm), proton beam, vertical betatron oscillations of amplitude 3 mm were excited by an inflector kick and the oscillation damping was observed (Figure 7). Use of the cooled proton beam enabled us to cancel the effect of proton-beam dimensions on damping time. This simplified significantly the interpretation of the results obtained.

The cooling-time dependence on the crossing angles between the proton orbit and electron beam axis is given in Figure 9. This is in good agreement with the results of numerical calculations simulating proton-beam cooling in NAP-M by an electron beam with a Maxwellian distribution of velocities. In Figure 9 the estimated curves $\tau(\theta_{r,z})$ are also given for various values of electron temperature. Experimental points fall closest to the estimated
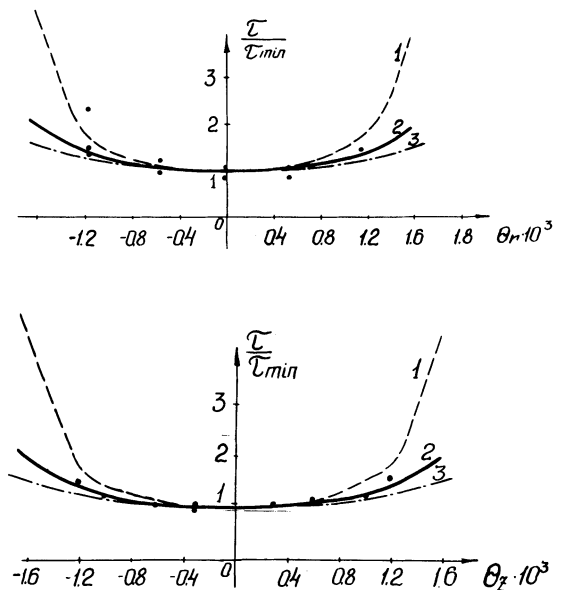

FIGURE 9 Cooling-time dependence of the proton-electron beam crossing angles. Experiment: 1 estimate for $\theta_e = 1.7 \times 10^{-3}$; 2—estimate for $\theta_e = 1.5 \times 10^{-3}$; 3—estimate for $\theta_e = 1.15 \times 10^{-3}$. Proton energy 65 MeV, electron current 100 mA.

curve corresponding to an electron temperature $T_e \simeq 0.2$ eV $(\theta_{er} \simeq \theta_{ez} \simeq 1.5 \times 10^{-3})$.

The cooling-time dependence on the initial amplitude value of betatron oscillations excited in the cooled beam was also measured (Figure 10). The decrement remains approximately constant up to an amplitude $A = 3$ mm $(\theta_p \simeq 2.5 \times 10^{-4})$. If the amplitude is larger than the electron-beam dimensions, the decrement reduces substantially, although cooling continues up to $A \simeq 1$ cm $(\theta_p \simeq 1.5 \times 10^{-3})$.
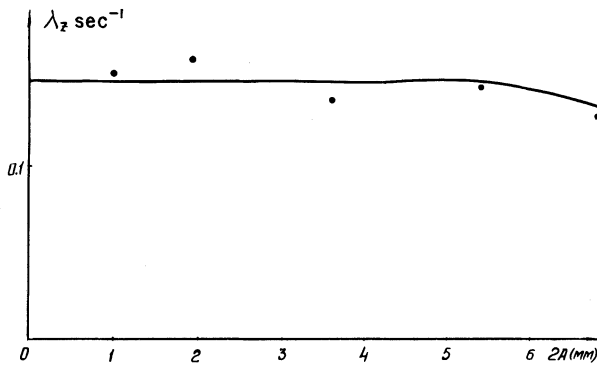

FIGURE 10   Cooling-time dependence on the initial amplitude of betatron oscillations excited in the cooled beam.

This result is consistent with measurements of the cooling-time dependence on the accuracy of the vertical coincidence of beams (Figure 11). In these experiments, the proton-beam shift with respect to the electron beam was performed by a proton-beam orbit displacement in the cooler straight section and the orbit-shift magnitude was measured by an aperture probe. The cooling time remained constant up to an orbit shift $\Delta z \simeq \pm 2$ mm. With larger shifts, the picture eventually became more
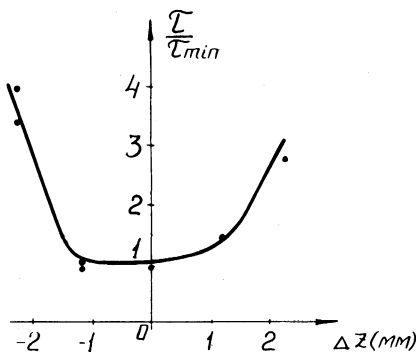

FIGURE 11   Cooling-time dependence on the distance between the beam axes. Proton energy 65 MeV, electron current 100 mA.
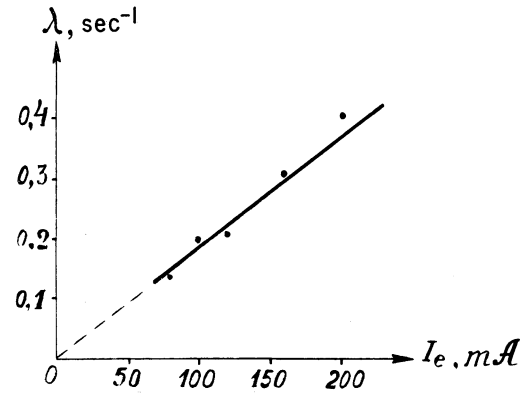

FIGURE 12   Dependence of the betatron-oscillation damping decrement on the electron current. Proton energy 65 MeV.

complicated due to electron-beam space-charge effects (Section VIII).

An orbit shift in radius does not affect the electron-cooling effectiveness unless the proton beam comes out of the electron beam.

Measurements of the cooling-time dependence on the electron current showed that within the range $I_e = 80\text{–}200$ mA, the decrement of oscillations increases linearly with the electron current (Figure 12), as the theory predicts. It is noticeable that even within this narrow range of current variations, the electron-beam space-charge influence was perceptible (see Section VIII).

For application of the method, it is essential to find out the cooling-time dependence on the mean particle energy. Corresponding measurements carried out within the proton energy region 35–75 MeV showed that τ_e increases with the energy growth approximately as β^2 ($j = $ const). This result can be interpreted as an increase of the effective temperature T_e with energy in Eq. (17).

VII   ENERGY-SPREAD DAMPING

In a way similar to Eqs. (12) and (14), one can obtain expressions for the momentum spread (monochromaticity) of a proton beam. One should now take into account, though, that due to electron acceleration the distribution function is substantially deformed. If near the electrode surface, the electron flux is sufficiently described by a quasi-Maxwellian distribution function of the velocities with the temperature equal to that of the cathode, after acceleration up to an energy W the longitudinal energy spread of electrons is reduced; as a result of this, the "longitudinal temperature" of

electrons in the particle system has the form

$$T_{\parallel} \simeq \frac{T_K^2}{2\gamma^2\beta^2mc^2} \rightarrow \frac{T_K^2}{4W}. \qquad (19)$$

This relation gives the nonrelativistic limit for the longitudinal temperature. From relation (19) it follows that the longitudinal temperature of the accelerated electron beam is substantially less than the transverse temperature. This condition is maintained because the time required for electrons to pass between the gun and collector is much less than that required for equalizing the temperatures of the different degrees of freedom.

If the mean electrode energy fluctuates with a frequency more than τ_e^{-1} (power-supply noise) then, of course, the effective temperature exceeds the value (19). This increase can be accounted for by adding the rms amplitude of the energy fluctuations

$$T_K^* = T_K + \Delta W. \qquad (20)$$

If the proton velocity spread in the particle system is much larger than that of longitudinal electron velocities in the same system, but less than the transverse velocity spread, or, in the laboratory system

$$\theta_{ei} \gg \frac{\Delta p}{p_s} \gg \frac{T_K^*}{\beta^2mc^2\gamma^2}, \qquad (21)$$

then in the laboratory system the temperature limit for the spread in the longitudinal component of proton momentum is described by the expression

$$\left(\frac{\Delta p}{p_s}\right)_{eq} \simeq \frac{m}{4M}\frac{L_{\perp}}{L_{\parallel}}\theta_{ei}. \qquad (22)$$

Here, $L_{\perp} \simeq L_p$, and $L_{\parallel}$ are, respectively, the Coulomb logarithms for the energy-transition processes in the particle system from the proton to electron in the transverse and longitudinal directions respectively in the presence of a longitudinal magnetic field.

If the limit (22) is so small that the equilibrium spread of the longitudinal proton velocities in the particle system is less than that for electrons, so that

$$\frac{m}{4M}\frac{L_{\perp}}{L_{\parallel}}\theta_{ei} < \frac{T_K^*}{\beta^2mc^2\gamma^2}, \qquad (23)$$

then the equilibrium spread $(\Delta p/p_s)_{eq}$ is

$$\left(\frac{\Delta p}{p_s}\right)_{eq} \simeq \sqrt{\frac{L_{\perp}}{L_{\parallel}}\theta_{el}\frac{T_K^*}{\beta^2mc^2\gamma}}. \qquad (24)$$

The beam monochromatization time required for the equilibrium value (22) is

$$\tau_{\parallel} \sim \frac{\tau_e}{\theta_{ei}}\left(\frac{\Delta p}{p}\right)_{in}\frac{L_{\perp}}{L_{\parallel}} \lesssim \tau_e. \qquad (25)$$

Here $(\Delta p/p_s)_{in}$ is the initial value for the proton momentum spread.

The cooling time and equilibrium amplitudes for betatron oscillations in the case of a flattened distribution are described by equations that differ from Eqs. (17), (12), and (14) only by numerical factors of order unity whose exact values depend on the specific form of the velocity distribution function for electrons.

The first experimental proof for proton momentum-spread damping due to electron cooling was the observation of the above-mentioned "blowing-off" effect. When the mean energy of electrons is changed within a small range close to its optimum value, the coasting proton beam is shifted in radius. This occurs because of the acceleration or deceleration of protons by electrons. It proceeds until the mean velocities of proton and electron beams become equal.

Figure 13 represents the oscillogram signals of the scintillation counter that registers protons scattered on the edge of the radial-aperture probe crossing the beam. If the electron energy is changed,

10.430
10.442
10.450
10.442-10.450

DIVIDER VOLTAGE
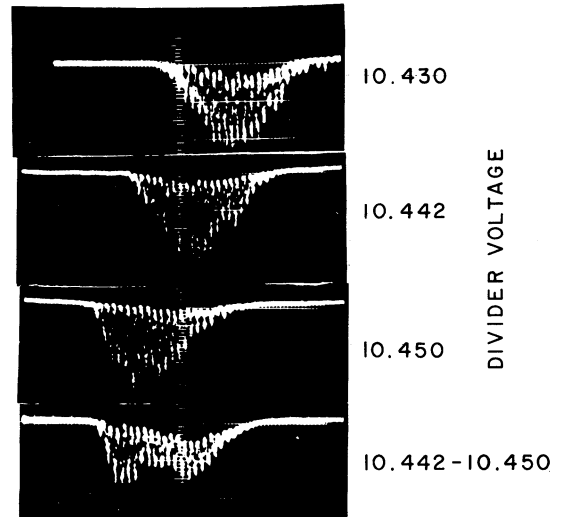
"VELOCITY ATTRACTION" BETWEEN ELECTRON AND PROTON BEAM

FIGURE 13 Proton beam "blowing off" by electron beam: dependence of the proton-beam shift in radius on electron energy. Proton energy 65 MeV, electron current 100 mA.

the signal center is shifted. The lower oscillogram demonstrates the partial "blowing-off" of protons with rapid (compared with $\tau_\parallel$) variation of electron energy for the value $\Delta W_e/W_e \simeq 8 \times 10^{-4}$. With poor pressure inside the electron device (5×10^{-9} Torr), the space charge of the electron beam is compensated by ions. A relation was obtained between the orbit displacement of protons and the relative variation of kinetic energy of electrons (Figure 14). Inside the electron beam the dependence is linear and consistent with the known value for the ψ function of the storage ring NAP-M in straight sections ($\psi = 0.8$).
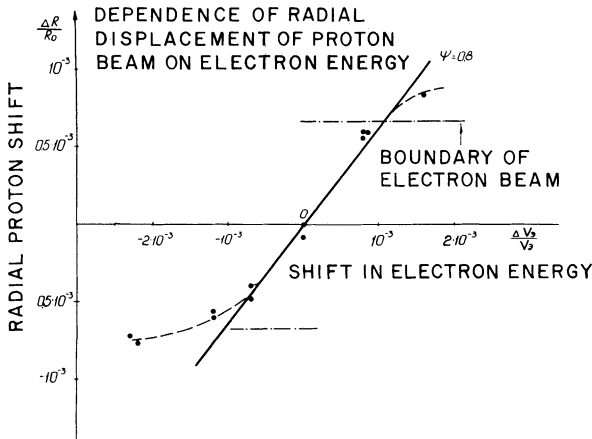
FIGURE 14   Dependence of the radial shift of a proton beam on electron energy when the mean velocities are close.

These results stimulated us to perform an experiment on proton acceleration by an electron beam. To this end, after switching cooling on, the electron energy and the magnetic field of the storage ring are increased simultaneously. The attainable proton energy gain was dependent on the correlation of the rates of variation of the storage-ring magnetic field and the electron energy. An optimum increase for the proton energy was found to be 1.2%, and the acceleration time was 200 sec, which corresponds to a mean rate of energy gain 4 keV/sec.

If one changes the electron energy suddenly and measures the speed of radial equilibrium-orbit displacement of the cooled proton beam, the longitudinal component of the friction force introduced by the electrons can be obtained.

$$\frac{1}{R_0}\frac{dR_0}{dt} = \frac{\psi}{p_s}F_\parallel. \qquad (26)$$
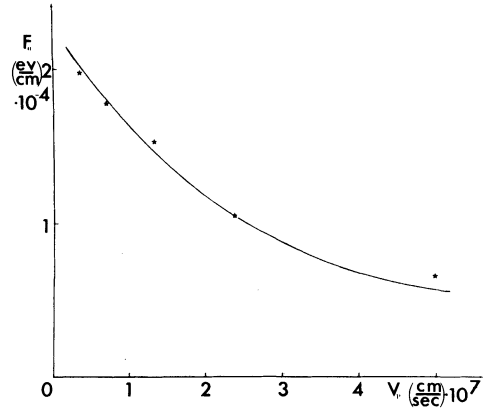
FIGURE 15   Longitudinal frictional-force dependence on the difference between the mean velocities of protons and electrons. Proton energy 65 MeV, electron current 100 mA.

In the experiments, whose results are shown in Figure 15, the time required for protons to reach the probe located at a distance 3 mm from the proton beam was measured. In Figure 15 in addition to experimental points, we show the calculated dependence $F_\parallel$ on the difference of mean velocities of protons and electrons, assuming a Maxwellian distribution of electrons in transverse velocities and a δ-function distribution in the longitudinal velocity. That is, $(T_\parallel \ll T_e)$. Values for transverse electron temperature and the Coulomb logarithm involved in $F_\parallel$ were obtained by employing the least squares method on the experimental data. These values are

$$T_e = 0.8 \text{ eV} (\theta_e \simeq 3.4 \times 10^{-3}), L_\parallel \simeq 8.$$

This difference between $L_\parallel$ and $L_\perp \simeq 20$ is apparently connected with the electron-beam "magnetization": the transition of proton energy to electrons is complicated by a magnetic field.

Direct measurements of the equilibrium value of the proton momentum spread were not carried out. If it is assumed that half of the proton-beam radial dimension is caused by the momentum spread, even then the value $(\Delta p/p_s)_{eq}$ does not exceed 5×10^{-5}. Estimates made with Eq. (21) for $\theta_e = 3.4 \times 10^{-3}$ and $\Delta W/W = 1 \times 10^{-4}$ give $(\Delta p/p_s)_{eq} \simeq 1 \times 10^{-5}$.

VIII   HIGH-CURRENT OPERATION

Experiments on electron cooling were started with relatively poor vacuum conditions, primarily because the vacuum chamber of the electron-beam

device was not designed to be heatable. As a result, even the small fraction of electron beam uncaptured by collector and striking the chamber walls caused intensive outgassing. After long training of the vacuum chamber by electrons, however, and reducing the electron-current losses to a level of $\Delta J_e/J_e \sim 8 \times 10^{-5}$, an average pressure 5×10^{-10} Torr was achieved with electron currents up to 250 mA.

With the vacuum improvement, the residual-gas concentration turned out to be insufficient to provide electron-beam space-charge neutralization, which was observed during measurements of the cooling-time dependence on the electron current value (see Section VI, Figure 12). When the electron current increases, the optimum energy value for cooling linearly increases so that

$$\frac{1}{J_e}\frac{\Delta W}{W} = 0.012 \text{ A}^{-1}. \tag{27}$$

This result enabled us to understand an effect produced by the electron-beam space charge on the cooling process. If the space charge is not compensated by residual-gas ions, the beam potential is reduced with respect to the vacuum-chamber walls by the value

$$\Delta U(\rho) = -\frac{J_e}{\beta c}\left(1 - \frac{\rho^2}{a_e^2} + 2\ln\frac{\rho_0}{a_e}\right), \tag{28}$$

where ρ is the distance from the beam axis and a_e and ρ_0 are the radii of the beam and chamber cross sections, respectively. This means that the electron energy is reduced by the same amount at the point ρ. Consequently, for resuming the cooling optimum it is necessary to increase the mean electron energy while increasing the current of electrons

$$\frac{1}{J_e}\frac{\Delta W}{W} = \frac{1 + 2\ln\dfrac{\rho_0}{a_e}}{\beta c W} = 0.011 \text{ A}^{-1} \tag{29}$$

which is in good agreement with the experimental results.

With good vacuum conditions, measurements were made of the cooling-time dependence τ_e on the electron-energy detuning (Figure 16). The allowable electron-energy deviation from its optimum value was found to be small; $\Delta W/W \simeq 5 \times 10^{-4}$. Direct measurements of the orbit distortion performed with the aperture probe gave the value $\Delta R \simeq \pm 3$ mm, which is twice the value that corresponds to the relative change of the proton
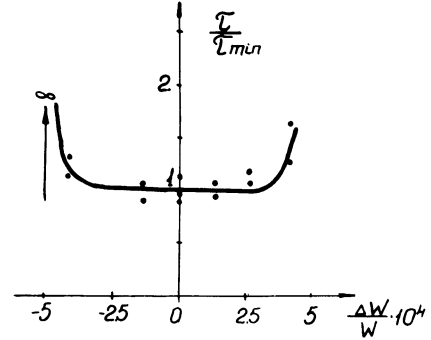

FIGURE 16 Dependence of the vertical betatron-oscillation damping time on the electron-energy detuning. Proton energy 65 MeV, electron current 100 mA.

energy (5×10^{-4}). This apparent disagreement is caused by electron-beam space-charge effects: according to Eq. (26), the energy of the electron beam depends on the distance from the beam axis. Therefore, when the mean energy of electrons $W(\rho = 0)$ is retuned, since the magnetic field is constant, the radius of the proton orbit is either increased or contracted decreased by the amount

$$\Delta R = \psi R_0 \frac{\Delta p(\Delta R)}{p_s} = \psi R_0 \frac{\Delta p_e(\Delta R)}{p_e}, \tag{30}$$

where p_e is the electron momentum on the beam axis and $\Delta p_e(\Delta R)$ is the difference in momentum between electrons off the axis and on the axis in accordance with Eq. (28).

Thus, under good vacuum conditions, when the space charge of an electron beam was not compensated, its effect was noticeable even at comparatively low electron current.

The influence of electron-beam density fluctuations on the cooling process was also studied. Electron density modulation was introduced by applying an alternating voltage ($\Delta V/V \simeq 10^{-2}$) to the first anode of the electron gun. At frequencies $\omega = (1 - v)\omega_0$, resonance excitation of betatron oscillations of protons was observed.

One more effect connected with ions accumulating inside the electron beam should be noted. Distributed ion pumps were located inside the vacuum chamber of the electron device. These pumps were designed for operation in the longitudinal magnetic field of the electron-beam device. It appears, though, that switching the electron beam on when the distributed pumps are in operation leads to a rapid loss of protons in a time much less than the proton lifetime without electron beam. Measurements of proton displacement showed

that in the electron beam, even at a current as small as $I_e = 10$ mA, charge is stored, producing an electric field of 300 V/cm. This accumulating charge is connected with the operation of the distributed pumps, where both neutral atoms and ions with an energy W_t of the level of 1 keV can be produced. Neutrals are ionized by the electron beam and leave it, leaving slow electrons "trapped" in the beam by the longitudinal magnetic field and the decelerating electric fields of the gun and collector at the beam ends. These electrons may leave the beam by diffusing slowly across the magnetic field or by recombination with ions. Accumulation of electrons proceeds until the fast ions are trapped by the negative beam potential produced by electrons, establishing the dynamic equilibrium between ionization and electrons leaving. As a result, the transverse electric field of stored electrons may achieve the value

$$E_\perp \sim \frac{W_i}{e\rho_0}. \tag{31}$$

The events led us to stop the use of distributed pumps during experiments and to design an improved vacuum chamber using distributed titanium sublimation pumps.

IX   CONCLUSION

The present work describes experimental studies of the main features of electron cooling. Good agreement with theoretical considerations was obtained.

The method developed opens up new possibilities in the physics of elementary particle and atomic nuclei:

1) Building of devices for proton-antiproton colliding beams of high luminosity at high and super-high energies. One of the possible projects of this kind is the project VAP-NAP at the Institute of Nuclear Physics of the Siberian Division, USSR Academy of Sciences, which is described in Ref. 4.

2) Building of a device with proton-antiproton colliding beams at an energy of some GeV with a very high monochromaticity (up to 10^{-6}) designed for precision experiments. Implied here are storage rings with built-in devices with electron beams, where electron cooling is not only employed for stacking antiprotons but also for maintaining the parameters of interacting colliding beams in the course of experiment.

3) Building of storage rings for protons, antiprotons, or multicharged ions of a very high monochromaticity for precision experiments on physics of atomic nuclei. In these accelerators, the particle beams are monochromatized with electron cooling before striking a target. Especially promising are such experiments with the use of internal super-thin targets. The thickness of such a target is limited by the condition suppressing multiple scattering of accelerated particles in the target by the electron-cooling effect.

4) Obtaining a large number of slow antiprotons for the study of scattering of antiprotons by nuclei and for the study of electromagnetic and nuclear-bound nucleon-antiproton states. Similar experiments can be set up with stacking of antiprotons of a low energy (on the level of MeV) and subsequent electrostatic deceleration. One can put the antiproton in an electromagnetically-bound state effectively by lining up the antiproton beam and a parallel beam of the required atoms with the same mean velocity. In these experiments, for electron cooling one will require an electron beam with a temperature T_e lower than that of a cathode.

5) Obtaining intense directed fluxes of antihydrogen (antiatoms) to carry out experiments on antiatom properties and for other exotic purposes. Antihydrogen generation may be performed using two storage rings (antiproton and positron) with common straight section where the particles have the same velocities.

The aim of this listing which, of course, does not cover all the possible applications of the method, is to call attention to its wide range.

REFERENCES

1. G. I. Budker, *Proc. Intern. Symp. on Electron and Positron Storage Rings*, Saclay, 1966, p. 11–1–1; *Atomnaya Energiya*, **22**, 346 (1967).
2. Ya. S. Derbenev, and A. N. Skrinsky, Kinetics of Electron Cooling, Preprint IYaF 225, Novosibirsk, 1968, unpublished.
3. G. I. Budker, Ya. S. Derbenev, N. S. Dikansky, V. V. Parchomchuk, D. V. Pestrikov, and A. N. Skrinsky, *Proc. 4th USSR National Conf. on Particle Accelerators, II*, Nauka 1975, p. 330.
4. Proton-antiproton colliding beams, VAPP-NAP Group Report in *Proc. 8th Intern. Conf. on High Energy Accelerators*, CERN 1971, p. 72.
5. G. I. Budker, N. S. Dikansky, V. I. Kudelainen, I. N. Meshkov, V. V. Parchomchuk, D. V. Pestrikov, A. N.

Skrinsky, and B. N. Sukhina, *Proc. 4th USSR National Conf. on Particle Accelerators, II*, Nauka 1975, p. 309.

6. G. I. Budker, Ya. S. Derbenev, N. S. Dikansky, V. I. Kudelainen, I. N. Meshkov, V. V. Parchomchuk, B. N. Sukhina, D. V. Pestrikov, and A. N. Skrinsky, *IEEE Trans. Nucl. Sci.*, **NS-20**, No. 5, 2093 (1975); *Atomnaya Energiya*, **40**, No. 1 (1976).

7. C. van der Meer, Report CERN/ISR-PO/70-5, 1970, unpublished.

8. C. van der Meer, Report CERN Int. Report, CERN/ISR/72-31, August 1972, unpublished.

9. P. Bramham, G. Carron, H. G. Hereward, K. Hühner, W. Schnell, and L. Thorndahl, *Nucl. Instrum. Methods*, **125**, 201 (1975).

10. V. V. Anashin, G. I. Budker, N. S. Dikansky, V. I. Kudelainen, A. S. Medvedko, I. N. Meshkov, V. V. Parchomchuk, D. V. Pestrikov, V. G. Ponomarenko, R. A. Salimov, A. N. Skrinsky, and B. N. Sukhina, *Proc. 4th USSR National Conf. on Particle Accelerators, II*, Nauka 1975, p. 304.

11. V. V. Anashin, G. I. Budker, and A. D. Bulushev *et al.*, Proton Storage Ring NAP-M. I. Magnetic and Vacuum Systems, Preprint IYaF 75-75, Novosibirsk, 1975, PTE (in print).

12. B. A. Baklakov and V. M. Borovikov *et al.*, Proton Storage Ring NAP-M. II. Current Stabilization for Supplying Guiding Field and Correction Coils, Preprint IYaF 75-76, Novosibirsk, 1976, PTE (in print).

13. V. F. Veremeenko and N. S. Dikansky *et al.*, Proton Storage Ring NAP-M. III. Accelerating System. Beam Monitoring, Preprint IYaF 75-77, Novosibirsk, 1975, PTE (in print).

14. Yu. A. Bolvanov and V. I. Kononov *et al.*, Proton Storage Ring NAP-M. IV. Storage Ring Control System, Preprint IYaF 75-78, Novosibirsk, 1975, PTE (in print).

15. G. I. Budker, V. I. Kudelainen, I. N. Meshkov, V. G. Ponomarenko, S. G. Popov, R. A. Salimov, A. N. Skrinsky, and B. M. Smirnov, *Proc. 2nd USSR National Conf. on Particle Accelerators, I*, 1972, p. 31.

16. V. I. Kudelainen, I. N. Meshkov, and R. A. Salimov, *JTF*, **11**, 2294 (1971).

17. B. A. Baklakov, V. F. Veremeenko, M. M. Karliner, A. A. Litvinov, and S. P. Petrov, Magnetomodulational Gauge of a Particle Beam Current, Preprint IYaF 74-40, Novosibirsk, 1974.

18. B. Vosicki and K. Zankel, *IEEE Trans. Nucl. Sci.*, **NS-22**, No. 3, 1475 (1975).

19. A. A. Kolomensky and A. N. Lebedev, *Cyclic Accelerator Theory*, Fizmatgiz (1962).

20. B. A. Trubnikov, *Problems of Plasma Theory*, Ed. I.M. (1963).